Non-coplanar trajectories to improve organ at risk sparing in volumetric modulated arc therapy for primary brain tumours

Gregory Smyth [1], Philip M. Evans [2], Jeffrey C. Bamber [1], Henry C. Mandeville [3], Liam C. Welsh [3], Frank H. Saran [3], James L. Bedford [1]

[1] Joint Department of Physics at The Institute of Cancer Research and The Royal Marsden NHS Foundation Trust, London, SM2 5PT, United Kingdom.

[2] Centre for Vision, Speech and Signal Processing, University of Surrey, Guildford, Surrey, GU2 7HX, United Kingdom.

[3] The Royal Marsden NHS Foundation Trust, London, SM2 5PT, United Kingdom.

Corresponding author: Gregory Smyth, Joint Department of Physics, The Institute of Cancer Research and The Royal Marsden NHS Foundation Trust, Downs Road, Sutton, London, SM2 5PT, United Kingdom. Email: greg.smyth@icr.ac.uk Tel: +44 20 8661 3472 Fax: +44 20 8643 3812

27 pages, 1 table, 5 figures

Running head: Non-coplanar trajectories for brain VMAT

Keywords: VMAT, non-coplanar, trajectory, optimization, treatment planning, hippocampal sparing

Abstract

Background and purpose: To evaluate non-coplanar volumetric modulated arc radiotherapy (VMAT) trajectories for organ at risk (OAR) sparing in primary brain tumour radiotherapy.

Materials and methods: Fifteen patients were planned using coplanar VMAT and compared against non-coplanar VMAT plans for three trajectory optimization techniques. A geometric heuristic technique (GH) combined beam scoring and Dijkstra's algorithm to minimize the importance-weighted sum of OAR volumes irradiated. Fluence optimization was used to perform a local search around coplanar and GH trajectories, producing fluence-based local search (FBLS) and FBLS+GH trajectories respectively.

Results: GH, FBLS, and FBLS+GH trajectories reduced doses to the contralateral globe, optic nerve, hippocampus, temporal lobe, and cochlea. However, FBLS increased dose to the ipsilateral lens, optic nerve and globe. Compared to GH, FBLS+GH increased dose to the ipsilateral temporal lobe and hippocampus, contralateral optics, and the brainstem and body. GH and FBLS+GH trajectories reduced bilateral hippocampi normal tissue complication probability ($p = 0.028$ and $p = 0.043$, respectively). All techniques reduced PTV conformity; GH and FBLS+GH trajectories reduced homogeneity but less so for FBLS+GH.

Conclusions: The geometric heuristic technique best spared OARs and reduced normal tissue complication probability, however incorporating fluence information into non-coplanar trajectory optimization maintained PTV homogeneity.

Introduction

Sparing organs at risk (OAR) in intracranial radiotherapy reduces the risk of side effects that affect quality of life, such as cranial and optic neuropathy, hearing loss, and neurocognitive impairment [1-6]. Using non-coplanar beam orientations has been shown to improve OAR dosimetry in conformal [7], intensity modulated (IMRT) [8], and volumetric modulated arc (VMAT) [9] radiation therapy. However, non-coplanar geometries are fixed during delivery for a given beam, limiting their application to VMAT. New linear accelerators can perform dynamic couch rotation during beam delivery, making possible non-coplanar VMAT trajectories that use more of the 4π space around the patient [10-12] and enabling potential additional reductions in normal tissue complication probability (NTCP).

Early research into the clinical benefit of non-coplanar VMAT mainly focused on planner-defined trajectories [13-15], while recent work has investigated trajectory optimization techniques [10, 16-19]. Published optimization techniques have used one of two approaches: geometric heuristics or fluence optimization. Geometric heuristics score individual beam orientations and determine trajectories that minimize the overall score [10, 16, 17]. Fluence-based techniques identify a smaller group of optimal candidate beam orientations, which are then connected via intermediate paths [18, 19]. Geometric heuristics are appealing due to the computational complexity of a full fluence search for a VMAT arc but lack the dosimetric information that can be utilized in fluence optimization.

This paper proposes and evaluates three different trajectory optimization techniques - a geometric heuristic technique and two incorporating fluence optimization - for primary brain tumour radiotherapy using non-coplanar VMAT. We aim to answer three questions:

1. Does a geometric heuristic technique improve OAR sparing over coplanar VMAT?

2. Does a fluence-based local search technique improve OAR sparing over coplanar VMAT?

3. Is there a synergistic effect if the geometric heuristic and fluence-based local search techniques are combined?

This work quantifies the clinical effect of new techniques for optimizing non-coplanar VMAT and aims to widen the therapeutic window of radiotherapy for primary brain tumours. We demonstrate that a less computationally intense geometric heuristic technique is sufficient to produce high quality plans. Our goal is to facilitate the introduction of non-coplanar VMAT into neuro-oncology clinical practice.

Materials and Methods

Patient selection and treatment planning

Fifteen patients treated with radiotherapy for primary brain tumours were planned using VMAT. Mean and standard deviation planning target volume (PTV) size was 336.6 ± 214.1 cc (range 5.5 – 723.6 cc), with a CTV-PTV margin of 3 mm in all cases. Original PTV prescription doses were 60 Gy in 2 Gy fractions, and 54 Gy or 59.4 Gy in 1.8 Gy fractions. One patient had palliative treatment (30 Gy in 6 Gy fractions) but was replanned to an appropriate radical dose (60 Gy in 2 Gy fractions) for this study. Further information for

each patient case is contained in Supplementary Table A1. Coplanar and non-coplanar radiotherapy plans were produced for a 6 MV Elekta Synergy linear accelerator (Elekta AB, Stockholm, Sweden) with Agility multi-leaf collimator [20]. Coplanar VMAT planning used our standard clinical technique of a single arc with 180 control points, however to avoid bias due to the additional degrees of freedom available to non-coplanar methods, dual arc coplanar plans with 360 control points were also produced.

Plans were optimized using an in-house VMAT planning system [21, 22] (AutoBeam v5.5a), adapted to import complex couch trajectories [16]. The planning process is summarized here, with the detailed workflow included in Supplementary Figure A1. AutoBeam performed fluence optimization at each control point before sequencing the fluence maps into deliverable connected VMAT apertures. As sequencing degraded the dose distribution, direct aperture optimization was performed subject to machine limits for VMAT delivery. Further detail on AutoBeam and the optimization techniques used at each stage can be found elsewhere [21, 22].

All cases used the same optimization objectives (Supplementary Table A2) to ensure a fair comparison. AutoBeam plans were reconstructed in Pinnacle^3 (Pinnacle^3 v9.8, Philips Medical, Madison, WI) for final dose calculation in line with clinical practice. Dose was prescribed to the PTV mean value and calculated on a 2.5 x 2.5 x 2.5 mm^3 resolution dose grid using the Adaptive Convolve algorithm.

Trajectory optimization

Three non-coplanar VMAT trajectory optimization techniques were developed in MATLAB (R2010b, The MathWorks, Natick, MA): a geometric heuristic technique (GH), a fluence-based local search technique (FBLS), and the combination of GH and FBLS (FBLS+GH). Organs at risk used in trajectory optimization were the brainstem, globes, optic nerves, optic chiasm, lenses, hippocampi, temporal lobes, cochleae, and the volume of brain excluding the PTV and other OARs. A patient voxel size of 5 x 5 x 5 mm^3 was used during trajectory optimization. For ray tracing, a beam aperture was defined as the projection of the PTV onto the isocentre plane and rays were cast through the centre of 2.5 x 2.5 mm^2 beam elements. A 2 mm margin was applied to the optic nerves, lenses, optic chiasm, and cochleae during trajectory optimization to prevent small OARs being missed in this step.

Geometric heuristic technique

The geometric heuristic technique (Figure 1(a)) is an extension of the algorithm described in [16]; further detail is provided in Supplementary Figure A1. Ray tracing was performed through the patient to determine a cost based on OAR geometry for all achievable isocentric beam orientations (Figure 1(a), step 1). The trajectory optimization was formulated as a graph search problem, with the cost for a given beam orientation being the penalty applied for adding that orientation to the VMAT trajectory, and solved using Dijkstra's least-cost path algorithm [23] (Figure 1(a), step 2). Single arc trajectories were produced through 358° of gantry rotation, from 179° to 181°, with control points spaced every 2° of gantry or couch rotation. Sections of trajectory with continuous couch rotation but static gantry rotation were allowed, provided the overall trajectory cost was minimised.

For this study the technique was extended to incorporate multiple OARs of different relative importance and prevent large or less important OARs from dominating the cost for a given beam orientation, a limitation of the previous method [16]. The cost, *C*, for each orientation is given by the sum of the relative volumes of each OAR intersected during ray tracing, weighted by their relative importance (Equation 1).

$$C_{c,g} = \sum_{v \in V} i_v \frac{n_v}{N_v} \qquad \text{Eq. 1}$$

where an OAR, *v*, from all clinically important OARs, *V*, with relative importance *i*, has *n* of *N* voxels intersected by rays cast from a beam orientation with couch angle, *c*, and gantry angle, *g*. The importance factors, *i*, were those used during plan optimization (Supplementary Table A2) and chosen based on relative clinical priority.

Fluence-based local search

One limitation of GH is that individual beam orientation costs, and therefore trajectories, do not evaluate the effect of fluence modulation around the arc. In some cases it may be beneficial to deliver dose to the PTV from beam angles which irradiate through an OAR, provided modulation is used to reduce the fluence directed at the OAR e.g. through the contralateral optics. GH would overlook these high cost beam orientations even if they might be included in a dosimetrically optimal trajectory. FBLS was developed to investigate the effect on plan dosimetry of local modifications, based on fluence modulation, to a supplied trajectory.

FBLS was applied to a coplanar VMAT trajectory to determine if it alone could significantly improve dosimetry. FBLS was also applied to a GH trajectory to investigate nearby

trajectories that, although not optimal in terms of geometric avoidance over the whole arc, might improve overall plan dosimetry.

FBLS algorithm

The FBLS algorithm (Figure 1(b)) is described below; further detail is provided in Supplementary Figure A1. The initial VMAT trajectory was downsampled to a 15-beam IMRT arrangement, approximately equispaced in gantry rotation (Figure 1(b), step 1). For each beam orientation, a simplified primary beam model [24] was used to map the influence of each ray, j, on the dose, D, to a patient voxel, i, according to Equation 2.

$$D_{ij} = \left(\frac{SID}{SSD + d} \right)^2 e^{-\mu d_w} \qquad \text{Eq. 2}$$

where SID is the source to isocentre distance, SSD is the source to patient surface distance, d is the depth of the calculation point, μ is the attenuation coefficient of water for a nominal 6 MV therapeutic beam (0.0495 cm^{-1}) and d_w is the water equivalent depth of the calculation point.

Fluence map optimization (FMO) was performed on the 15-beam IMRT plan to characterise the dosimetry of the VMAT trajectory with a similar resolution to Bzdusek et al. [25] for coplanar VMAT planning. FMO proceeded for 30 iterations of iterative least squares [21] using the clinical treatment planning objectives (Supplementary Table A2). The deviation of each objective, weighted by its corresponding importance factor, was determined and then summed to form a local search objective function.

The couch rotation of the first beam orientation was perturbed by a step size of ±10°, with new FMO performed, and the change that most improved the objective function was accepted (Figure 1(b), step 2). For each beam in turn, repeated perturbations were performed and accepted until there was no absolute improvement in the objective function from adjusting the current beam (Figure 1(b), step 3). The perturbation step size was then reduced incrementally from 10° to 2° and the perturbation stage repeated for each beam at its new couch angle (Figure 1(b), step 4). The set of all new beam orientations was then incorporated into the original trajectory using MATLAB's piecewise cubic hermite polynomial interpolation [26]. Checks were performed to ensure the interpolated trajectory avoided collision regions and did not extend beyond the initial arc start and stop gantry angles. Finally, the trajectory was resampled to maintain the same number of control points as the input trajectory (Figure 1(b), step 5).

Plan evaluation

Dose statistics were compared for all plans, with OAR doses judged against relevant QUANTEC constraints [1]. Dose-volume statistics linked to cognitive performance, V_{10Gy} and V_{40Gy} for the hippocampi, and V_{40Gy} and V_{60Gy} for the temporal lobes [27], were also compared. The probability of radiation induced cognitive impairment, as measured by the Wechsler Memory Scale-III Word List Delayed Recall (WMS-III WL-DR) test, was calculated from the equivalent dose in 2 Gy fractions to 40% of the bilateral hippocampi (EQD_2 40%) according to the NTCP model proposed by Gondi *et al.* [6]. All plans were compared against monitor units required, homogeneity index [28] (HI):

$$HI = \frac{D_{2\%} - D_{98\%}}{D_{50\%}} \times 100 \qquad \text{Eq. 3}$$

where $D_{2\%}$, $D_{98\%}$ and $D_{50\%}$ are the doses to 2 %, 98 % and 50 % of the PTV respectively,

van't Riet's conformation number [29] (CN):

$$CN = \frac{V_{T,95\%}}{V_T} \times \frac{V_{T,95\%}}{V_{95\%}} \quad \text{Eq. 4}$$

where V_T is the volume of the PTV, $V_{95\%}$ is the volume of the 95 % isodose, and $V_{T,95\%}$ is the volume of the PTV encompassed by the 95 % isodose,

and gradient index (GI):

$$GI = \frac{V_{50\%}}{V_{95\%}} \quad \text{Eq. 5}$$

where $V_{50\%}$ and $V_{95\%}$ are the volumes of the 50 % and 95 % isodoses respectively.

Statistical analysis was performed using a two-tailed Wilcoxon signed-rank matched-pairs test in SPSS (v22, IBM Corporation, Armonk, New York), with comparisons judged significant if $p < 0.05$. Single and dual arc coplanar VMAT were compared to determine if adding additional control points significantly improved the plans produced. All three non-coplanar techniques were compared with coplanar VMAT. The effect of combining the two optimization approaches was determined by comparing GH with FBLS+GH.

Results

Dual arc coplanar plans were not significantly different from single arc coplanar for most metrics studied (Supplementary Table A3). However, the contralateral optic nerve, hippocampus and temporal lobe, and body excluding PTV dose statistics and gradient index showed modest improvements. In all cases where metrics were improved by dual arc planning, statistical significance tests against non-coplanar VMAT were unaffected by the number of coplanar arcs. As the number of control points used for single arc coplanar plans (180) was similar to non-coplanar plans (median 180, range 180 – 202 for GH and FBLS+GH; 180 for FBLS), remaining comparisons are against single arc coplanar VMAT only.

Coronal sections through all plans for a representative patient case are presented in Figure 2. Note how the orientation of the isodose levels in the non-coplanar plans differs from the coplanar case to avoid the OARs, particularly for the 50 % and 20 % isodoses. Trajectories for all plans for one patient case are shown in Figure 3 overlaid on the cost map of the geometric heuristic technique. Regions of the cost map with high cost indicate beam orientations where a large proportion of clinically important organs at risk would be irradiated by a beam aperture conforming to the projection of the PTV. Low cost regions indicate beam orientations where no OARs, or a small proportion of low importance OARs, would be irradiated. Potential collision regions, estimated with a volunteer lying on the treatment couch, are shown in white.

Mean relative dose or volume deviations of clinically relevant OAR statistics from the coplanar VMAT plan are presented in Figure 4, with negative values indicating reductions and error bars indicating ±1 standard deviation. Complete results, including absolute dose

statistics and statistical comparisons, are presented in Table 1. All three non-coplanar trajectory optimization techniques significantly reduced doses to the contralateral globe, optic nerve, hippocampus (mean dose and V_{40Gy}), temporal lobe (mean dose and V_{40Gy}), and cochlea. Additionally GH and FBLS+GH significantly reduced the contralateral lens dose and contralateral hippocampus V_{10Gy}; GH also reduced the mean brainstem dose. FBLS significantly increased doses to the ipsilateral globe, optic nerve (mean), and lens. Compared to GH, FBLS+GH significantly increased dose to the brainstem, contralateral optics, ipsilateral hippocampus (mean dose and V_{40Gy}), ipsilateral temporal lobe (mean), and body excluding PTV.

PTV homogeneity index increased for GH ($p = 0.004$) and FBLS+GH ($p = 0.013$) plans compared with coplanar VMAT. However, FBLS+GH improved homogeneity over GH ($p = 0.009$). PTV coverage was less conformal for GH ($p = 0.033$), FBLS ($p = 0.002$), and FBLS+GH ($p = 0.015$) compared with coplanar VMAT. Gradient index was improved by FBLS ($p = 0.001$) and FBLS+GH ($p = 0.029$) plans compared with coplanar; FBLS+GH plans also improved over GH ($p = 0.004$). Non-coplanar plans required more monitor units than coplanar VMAT ($p = 0.001$ for all techniques) but there was no difference between GH and FBLS+GH.

Predicted clinical effect

Whole body D_{1cc} to patients with 59.4 Gy and 60 Gy prescriptions exceeded 60 Gy for all techniques (maximum 63.5 Gy), suggesting a risk of brain necrosis of 3-5 % [2]. Although non-coplanar techniques showed small increases in D_{1cc}, these are unlikely to result in

clinically significant differences in symptomatic necrosis risk. No patient received 59 Gy to more than 10 cc of the brainstem, complying with QUANTEC constraints [1].

QUANTEC optic nerve or chiasm constraints (maximum dose < 55 Gy) were exceeded in eight patients. Constraints were exceeded for the ipsilateral optic nerve in four patients, and the contralateral optic nerve in one patient, for all coplanar and non-coplanar plans. For patient 2, the ipsilateral optic nerve maximum dose increased to 55.3 Gy for GH from 54.8 Gy for coplanar VMAT, but reduced to 54.4 Gy with FBLS+GH. Seven patients exceeded the optic chiasm constraint, of which five exceeded the constraint for all coplanar and non-coplanar plans. For patient 4, the maximum chiasm dose increased to 56.6 Gy and 55.8 Gy for GH and FBLS+GH respectively from the initial coplanar VMAT dose of 54.4 Gy. For patient 6, the maximum chiasm dose was reduced to below the constraint for all non-coplanar plans from the initial coplanar VMAT dose of 55.1 Gy. QUANTEC suggests the threshold for optic neuropathy may be 59 Gy for non-pituitary tumours at these fraction sizes [4]. One case with a prescription dose of 60 Gy (patient 8) exceeded 59 Gy to the ipsilateral optic nerve and chiasm; this was breached for all plans including coplanar VMAT. None of these changes in dose would be expected to significantly affect the likelihood of radiation induced optic neuropathy.

There was no difference in the number of patients breaching the QUANTEC cochlear dose constraints between techniques at either the standard 45 Gy or conservative 35 Gy levels, corresponding to a 30 % chance of hearing loss. However, the significant reduction in contralateral cochlear dose demonstrated by the non-coplanar techniques could reduce the likelihood of hearing loss.

Dose volume histograms (DVH) of the contralateral hippocampus and temporal lobe for three representative patient cases are shown in Figure 5. Contralateral hippocampus and temporal lobe V_{40Gy} were significantly reduced by all non-coplanar techniques, while contralateral hippocampus V_{10Gy} was reduced by GH and FBLS+GH. Median overlap of the bilateral hippocampi with the PTV was 29.2 % (range 0 - 59.5 %), with six patients having an overlap of more than 40 %. The probability of cognitive impairment for GH plans (mean ± 1 S.D., 0.875 ± 0.263) was significantly reduced from coplanar VMAT (0.936 ± 0.183, $p = 0.028$). FBLS+GH significantly increased cognitive impairment probability (0.898 ± 0.229, $p = 0.028$) over GH, but remained significantly reduced over coplanar VMAT ($p = 0.043$).

Discussion

This work evaluates three non-coplanar VMAT trajectory optimization techniques for a cohort of primary brain tumour patients. Having performed a systematic comparison of these techniques, alone and in combination, we can draw some specific conclusions regarding their relative merits. FBLS achieved additional contralateral OAR sparing over coplanar VMAT plan, while maintaining PTV homogeneity, but increased dose to ipsilateral OARs. FBLS+GH maintained much of the OAR sparing of GH while recovering some lost PTV dose homogeneity. The trade-off between PTV dose homogeneity and OAR sparing depends on the planning objectives used, while the extent to which individual OARs are spared depends on their relative importance for the specific clinical case. For this cohort, it is important to maximize OAR sparing and therefore the geometric heuristic technique is recommended for primary brain tumours.

Recent work has proposed different heuristic or fluence-based methods of trajectory optimization [10, 16-19]. Fluence-based techniques solved non-coplanar IMRT beam orientation problems for up to 20 beams but did not evaluate the dosimetry of the connecting paths [18, 19]; therefore the final VMAT trajectories may not be globally optimal. FBLS accepted only local changes that decreased the local search objective function and therefore did not guarantee the altered VMAT trajectory was optimal. However, it did allow the dosimetry of alternate trajectories to be investigated while maintaining the quality of the rest of the connected trajectory. The complexity of FBLS was limited by using a simplified beam model; further work to incorporate a clinical dose model and determine its effect on trajectory optimization is planned.

More general issues regarding the potential clinical implementation of dynamic couch non-coplanar VMAT have yet to be fully addressed. While modern linear accelerators can deliver non-coplanar VMAT [10, 17], there has been no systematic investigation of its delivery accuracy or efficiency. Although statistically significant, coplanar and non-coplanar monitor units were sufficiently similar that we expect delivery efficiency to depend on couch rotation speed. Potential differences in delivery efficiency between non-coplanar trajectories will depend on gantry rotation, couch rotation, and dose rate limits for the specific machine. Dynamic couch rotation requires extra quality assurance testing [30] and advanced collision prediction and detection methods [31]. Patient rotation during treatment could introduce intra-fractional motion, with the effect dependent on treatment site and couch trajectory. Although additional immobilization is unlikely to be necessary for intracranial treatments, this may be a significant issue for other body sites and requires investigation. An alternative

linac configuration capable of rotation around the vertical axis allows non-coplanar treatment without patient movement and would address some of these problems [32, 33]. However, the reduced range of rotation achievable [32] may limit the utility of this approach for intracranial sites. The trajectory optimization techniques described in this work are applicable to all delivery platforms, within machine limitations.

Non-coplanar VMAT demonstrated improved sparing of functionally important OARs, notably significantly decreasing dose to the contralateral temporal lobe and hippocampus (Figure 5). Neurocognitive decline has been linked to higher doses to the hippocampi [6, 27, 34, 35] and temporal lobes [27, 34, 36]. Redmond *et al.* found reductions in children's motor speed and dexterity were correlated with increased dose to the hippocampi and temporal lobes, while visual perception decreased with increasing dose to the left temporal lobe [34]. Jalili *et al.* found children and young adults receiving greater than 43.2 Gy to 13 % of the left temporal lobe were significantly more likely to demonstrate a reduction in intelligence quotient (IQ) of 10 % or more [36]. The effect of hippocampal sparing in whole brain radiotherapy is currently under active investigation in several clinical trials worldwide, and has shown promising results in the RTOG 0933 phase 2 trial [35]. Gondi *et al.* modelled the probability of impaired learned-word recall with increasing dose to the hippocampi for a cohort of adult patients [6]. Gondi *et al.*'s NTCP model of cognitive injury due to hippocampal dose results in a rather stringent hippocampal dose sparing requirement ($D_{40\%}$ to the bilateral hippocampi leading to a 50% probability of WMS-III WL-DR impairment (EQD^{50}_{2}) was estimated to be 14.88 Gy [95% CI, 12.86-17.06 Gy]) that may be difficult to achieve in practice for patients treated for primary brain tumours where intra-cranial tumour control is the priority. While the modelled hippocampal NTCP reductions achieved by non-coplanar VMAT were modest, the absolute dose reductions achieved for the contralateral

temporal lobe and hippocampus (Figure 5) are likely to be clinically significant [27]. These studies suggest that non-coplanar VMAT using dynamic couch rotation should reduce the incidence and severity of neurocognitive side effects by limiting dose to the contralateral temporal lobe and hippocampus. The potential benefit of non-coplanar VMAT for a homogeneous cohort of primary brain tumour patients should now be evaluated within a clinical trial.

Conclusions

Non-coplanar VMAT trajectories using GH significantly spared contralateral OARs over coplanar VMAT for primary brain tumours. Both fluence-based trajectories emphasized PTV homogeneity over OAR sparing, although FBLS+GH maintained most of the OAR sparing achieved by GH. However, for primary brain tumour patients, organ at risk sparing is clinically more important than the relatively small differences in PTV homogeneity. Therefore, non-coplanar VMAT using the geometric heuristic technique is recommended to reduce normal tissue complication probability for primary brain tumour patients.

Conflict of interest statement

JCB reports grants from Cancer Research UK, grants from NHS funding to the NIHR Biomedical Research Center at The Royal Marsden and the ICR, during the conduct of the study. JLB reports grants, non-financial support and other from Elekta AB (Stockholm), outside the submitted work. GS, LCW, HCM, FHS and PME have nothing to disclose.

Acknowledgements

The authors thank Dr Simona Gaito for assistance with organ at risk delineation. We are grateful for NHS funding to the NIHR Biomedical Research Centre at The Royal Marsden and The Institute of Cancer Research. Research at The Institute of Cancer Research is also supported by Cancer Research UK under Programs C46/A10588 and C33589/A19727.

References

[1] Jackson A, Marks L B, Bentzen S M et al. The lessons of QUANTEC: recommendations for reporting and gathering data on dose–volume dependencies of treatment outcome. Int. J. Radiat. Oncol. Biol. 2010; 76: S155-60.

[2] Lawrence Y R, Li X A, El Naqa I et al. Radiation dose–volume effects in the brain. Int. J. Radiat. Oncol. Biol. 2010; 76: S20-7

[3] Mayo C, Yorke E, Merchant T E. Radiation associated brainstem injury. Int. J. Radiat. Oncol. Biol. 2010; 76: S36-41.

[4] Mayo C, Martel M K, Marks L B, Flickinger J, Nam J, Kirkpatrick J. Radiation dose–volume effects of optic nerves and chiasm. Int. J. Radiat. Oncol. Biol. 2010; 76: S28-35.

[5] Bhandare N, Jackson A, Eisbruch A et al. Radiation therapy and hearing loss. Int. J. Radiat. Oncol. Biol. 2010; 76: S50-7.

[6] Gondi V, Hermann B P, Mehta M P, Tomé W A. Hippocampal dosimetry predicts neurocognitive function impairment after fractionated stereotactic radiotherapy for benign or low-grade adult brain tumours. Int. J. Radiat. Oncol. Biol. Phys. 2013; 85: 348-54

[7] Rowbottom C G, Oldham, M Webb S. Constrained customization of non-coplanar beam orientations in radiotherapy of brain tumours. Phys. Med. Biol. 1999; 44: 383.

[8] Bangert M, Ziegenhein Z, Oelfke U. Comparison of beam angle selection strategies for intracranial IMRT. Med. Phys. 2013; 40: 011706.

[9] Beltran C, Gray J, Merchant T E. Intensity-modulated arc therapy for pediatric posterior fossa tumours. Int. J. Radiat. Oncol. Biol. 2012; 82: e299-304.

[10] Yang Y, Zhang P, Happersett L et al. Choreographing couch and collimator in volumetric modulated arc therapy. Int. J. Radiat. Oncol. Biol. Phys. 2011; 80: 1238–47.

[11] Fahimian B, Yu V, Horst K, Xing L, Hristov D. Trajectory modulated prone breast irradiation: A linac-based technique combining intensity modulated delivery and motion of the couch. Radiother. Oncol. 2013; 109: 475–81.

[12] Dong P, Lee P, Ruan D et al. 4π non-coplanar liver SBRT: A novel delivery technique. Int. J. Radiat. Oncol. Biol. Phys. 2013; 85: 1360-6.

[13] Krayenbuehl J, Davis J B, Ciernik I F. Dynamic intensity-modulated non-coplanar arc radiotherapy (INCA) for head and neck cancer. Radiother. Oncol. 2006; 81: 151-7.

[14] Shaitelman S F, Kim L H, Yan D, Martinez A A, Vicini F A, Grills I S. Continuous arc rotation of the couch therapy for the delivery of accelerated partial breast irradiation: a treatment planning analysis. Int. J. Radiat. Oncol. Biol. Phys. 2011; 80: 771-8

[15] Popescu C C, Beckham W A, Patenaude V V, Olivotto I A, Vlachaki M T. Simultaneous couch and gantry dynamic arc rotation (CG-DARC) in the treatment of breast cancer with accelerated partial breast irradiation (APBI): a feasibility study. J. Appl. Clin. Med. Phys. 2013; 14: 161–75.

[16] Smyth G, Bamber J C, Evans P M, Bedford J L. Trajectory optimisation for dynamic couch rotation during volumetric modulated arc radiotherapy. Phys. Med. Biol. 2013; 58: 8163–77.

[17] MacDonald R L, Thomas C G. Dynamic trajectory-based couch motion for improvement of radiation therapy trajectories in cranial SRT. Med. Phys. 2015; 42: 2317-25

[18] Wild E, Bangert M, Nill S, Oelfke U. Noncoplanar VMAT for nasopharyngeal tumours: Plan quality versus treatment time. Med. Phys. 2015; 42: 2157-68.

[19] Papp D, Bortfeld T, Unkelbach J. A modular approach to intensity-modulated arc therapy optimization with noncoplanar trajectories. Phys. Med. Biol. 2015; 60: 5179

[20] Bedford J L, Thomas M D, Smyth G. Beam modeling and VMAT performance with the Agility 160-leaf multileaf collimator. J. Appl. Clin. Med. Phys. 2013; 14: 172-85

[21] Bedford J L. Treatment planning for volumetric modulated arc therapy. Med. Phys. 2009; 36: 5128–38.

[22] Bedford J L. Sinogram analysis of aperture optimization by iterative least-squares in volumetric modulated arc therapy. Phys. Med. Biol. 2013; 58: 1235–50.

[23] Dijkstra E W. A note on two problems in connexion with graphs. Numer. Math. 1959; 1: 269–71.

[24] Rowbottom C G, Webb S, Oldham M. Improvements in prostate radiotherapy from the customization of beam directions. Med. Phys. 1998; 25: 1171-9.

[25] Bzdusek K, Friberger H, Eriksson K, Hårdemark B, Robinson D, Kaus M. Development and evaluation of an efficient approach to volumetric arc therapy planning. Med. Phys. 2009; 36: 2328-39.

[26] Fritsch F N, Carlson R E. Monotone piecewise cubic interpolation. SIAM J. Numer. Anal. 1980;17: 238-46.

[27] Peiffer A M, Leyrer C M, Greene-Schloesser D M et al. Neuroanatomical target theory as a predictive model for radiation-induced cognitive decline. Neurology 2013; 80: 747-53

[28] The International Commission on Radiation Units and Measurements. Prescribing, Recording, and Reporting Intensity-Modulated Photon-Beam Therapy (IMRT). ICRU Report 83. J ICRU 2010;10

[29] Van't Riet A, Mak A C, Moerland M A, Elders L H, van der Zee W. A conformation number to quantify the degree of conformality in brachytherapy and external beam irradiation: application to the prostate. Int. J. Radiat. Oncol. Biol. Phys. 1997; 37: 731-6

[30] Yu V Y, Fahimian B P, Xing L, Hristov D H. Quality control procedures for dynamic treatment delivery techniques involving couch motion. Med. Phys. 2014; 41: 081712.

[31] Yu V Y, Tran A, Nguyen D et al. The development and verification of a highly accurate collision prediction model for automated noncoplanar plan delivery. Med. Phys. 2015; 42: 6457-67.

[32] Mizowaki T, Takayama K, Nagano K et al. Feasibility evaluation of a new irradiation technique: three-dimensional unicursal irradiation with the VERO4DRT (MHI-TM2000). J. Radiat. Res. 2013; 54: 330–6.

[33] Burghelea M, Verellen D, Poels K et al. Geometric verification of Dynamic Wave Arc delivery with the Vero system using orthogonal X-ray fluoroscopic imaging. Int. J. Radiat. Oncol. Biol. Phys. 2015; 92: 754–61.

[34] Redmond K J, Mahone E M, Terezakis S et al. Association between radiation dose to neuronal progenitor cell niches and temporal lobes on performance on neuropsychological testing in children: a prospective study. Neuro. Oncol. 2013; 15: 360-9

[35] Gondi V, Pugh S L, Tome W A, Caine C et al. Preservation of memory with conformal avoidance of the hippocampal neural stem-cell compartment during whole-brain radiotherapy for brain metastases (RTOG 0933): a phase II multi-institutional trial. 2014; 32: 3810-6

[36] Jalili R, Mallick I, Dutta D et al. Factors influencing neurocognitive outcomes in young patients with benign and low-grade brain tumours treated with stereotactic conformal radiotherapy. Int. J. Radiat. Oncol. Biol. Phys. 2010;77:974-9

Table 1. Mean and standard deviations of dose statistics for coplanar and geometric heuristic technique (GH), fluence-based local search (FBLS), and combined GH and FBLS (FBLS+GH) non-coplanar VMAT trajectories. Significant statistical comparisons ($p < 0.05$) are indicated as follows: (a) coplanar vs GH, (b) coplanar vs FBLS, (c) coplanar vs FBLS+GH, (d) GH vs FBLS+GH, (e) GH vs FBLS, (f) FBLS vs FBLS+GH. Ipsi and contra = ipsilateral and contralateral. Dx = dose to volume x. VxGy = relative volume receiving x Gy.

Figure 1. Non-coplanar trajectory optimization methods for (a) the geometric heuristic technique (GH), and (b) the fluence-based local search (FBLS) algorithm. Followed left to right, (b) shows how the FBLS algorithm updates at each numbered step. As the example shown uses GH as its initial trajectory, (b) would produce a FBLS+GH trajectory. All trajectories are overlaid on the normalised GH cost map. White regions indicate excluded potential collision regions; high cost regions indicate orientations where a beam aperture conforming to the PTV would irradiate multiple or high importance organs at risk. In (b), black and grey circles indicate current and previously considered beam orientations respectively; the dashed line indicates the new trajectory.

Figure 2. Coronal sections for Case 4, showing plans for (a) coplanar VMAT, (b) the geometric heuristic technique (GH), (c) the fluence-based local search (FBLS), and (d) the combination of GH and FBLS (FBLS+GH). PTV (pink colorwash), hippocampus (orange),

temporal lobe (yellow), brainstem (red), and cochlea (purple) are shown. Isodose lines are 95% (green), 80% (blue), 50% (lilac), and 20% (brown) of prescription dose.

Figure 3. VMAT trajectories for (a) the geometric heuristic technique (GH), (b) fluence-based local search (FBLS), and (c) and the combination of GH and FBLS (FBLS+GH). All trajectories are overlaid on the normalised cost map for the geometric heuristic technique. White regions indicate excluded potential collision regions; high cost regions indicate orientations where a beam aperture conforming to the PTV would irradiate multiple or high importance organs at risk.

Figure 4. Mean relative deviations from single arc VMAT of clinically relevant organ at risk (a) maximum dose, (b) mean dose, and (c) dose volume statistics for the geometric heuristic technique (GH), fluence-based local search (FBLS), and combined GH and FBLS (FBLS+GH). Error bars show ± 1 standard deviation. Vx = relative volume receiving x Gy; I. = ipsilateral; C. = contralateral; temp. = temporal lobe; hippo. = hippocampus.

Figure 5. PTV and contralateral hippocampus (a, c, e) and contralateral temporal lobe (b, d, f) dose volume histograms for the geometric heuristic technique (GH), fluence-based local search (FBLS), and combined GH and FBLS (FBLS+GH), for representative patient cases with small (top; Case 1), medium (middle; Case 9), and large (bottom; Case 15) PTV volumes.

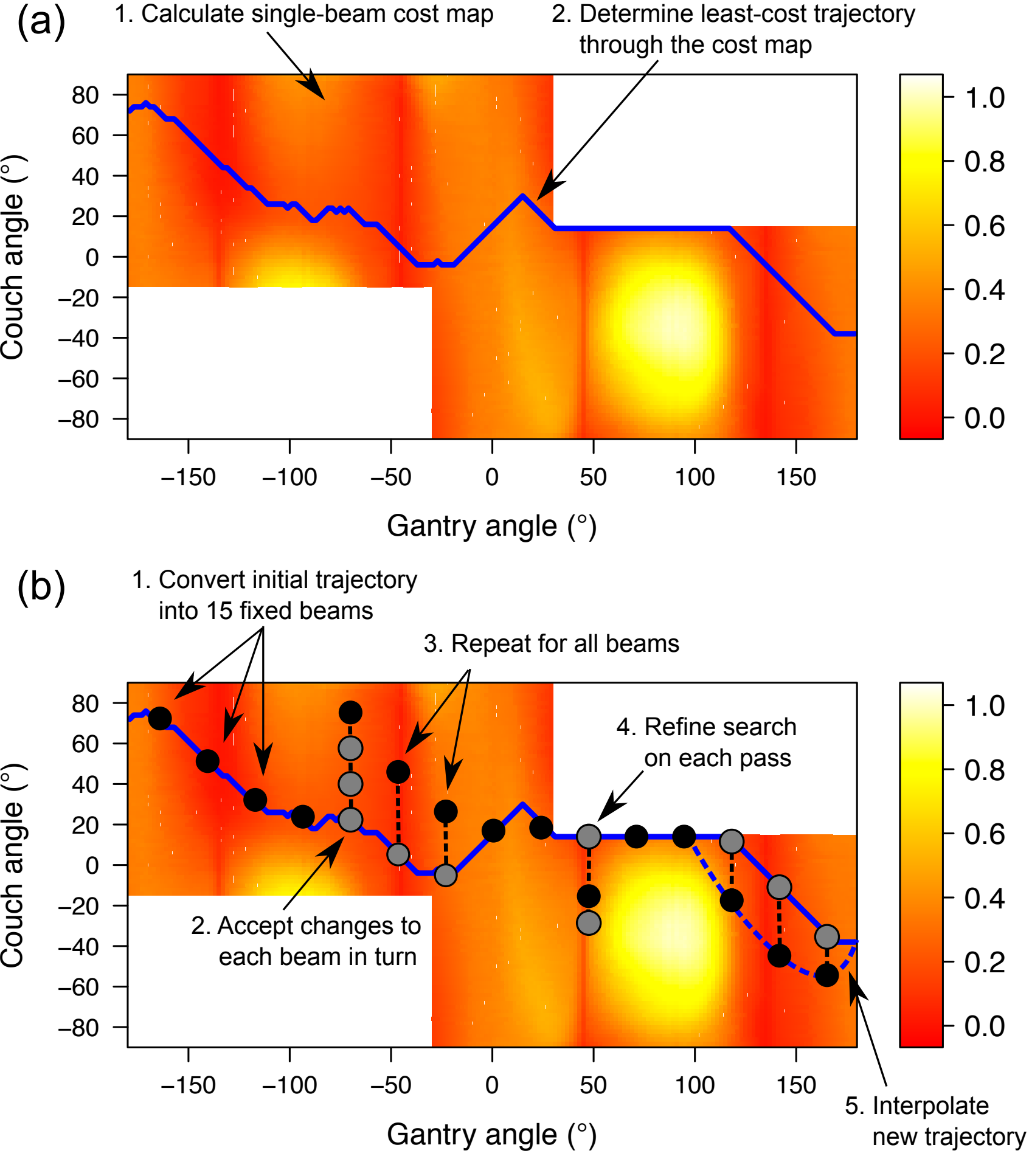
(a)
1. Calculate single-beam cost map
2. Determine least-cost trajectory through the cost map
Couch angle (°)
80
60
40
20
0
−20
−40
−60
−80
−150
−100
−50
0
50
100
150
Gantry angle (°)
1.0
0.8
0.6
0.4
0.2
0.0
(b)
1. Convert initial trajectory into 15 fixed beams
3. Repeat for all beams
4. Refine search on each pass
2. Accept changes to each beam in turn
5. Interpolate new trajectory
Couch angle (°)
Gantry angle (°)

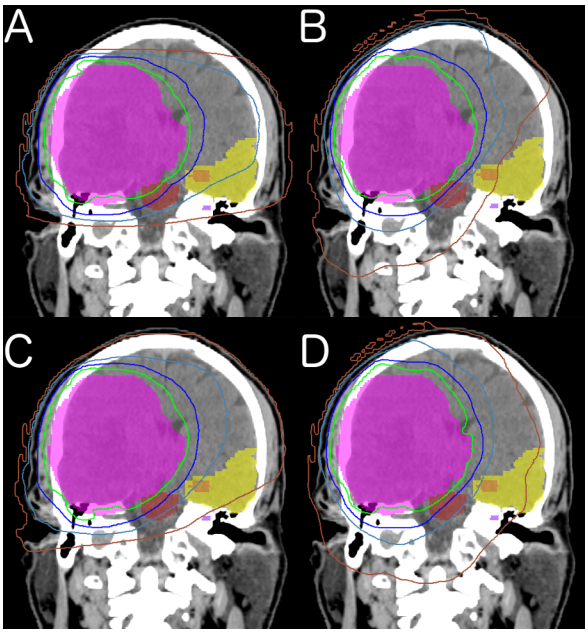
A
B
C
D

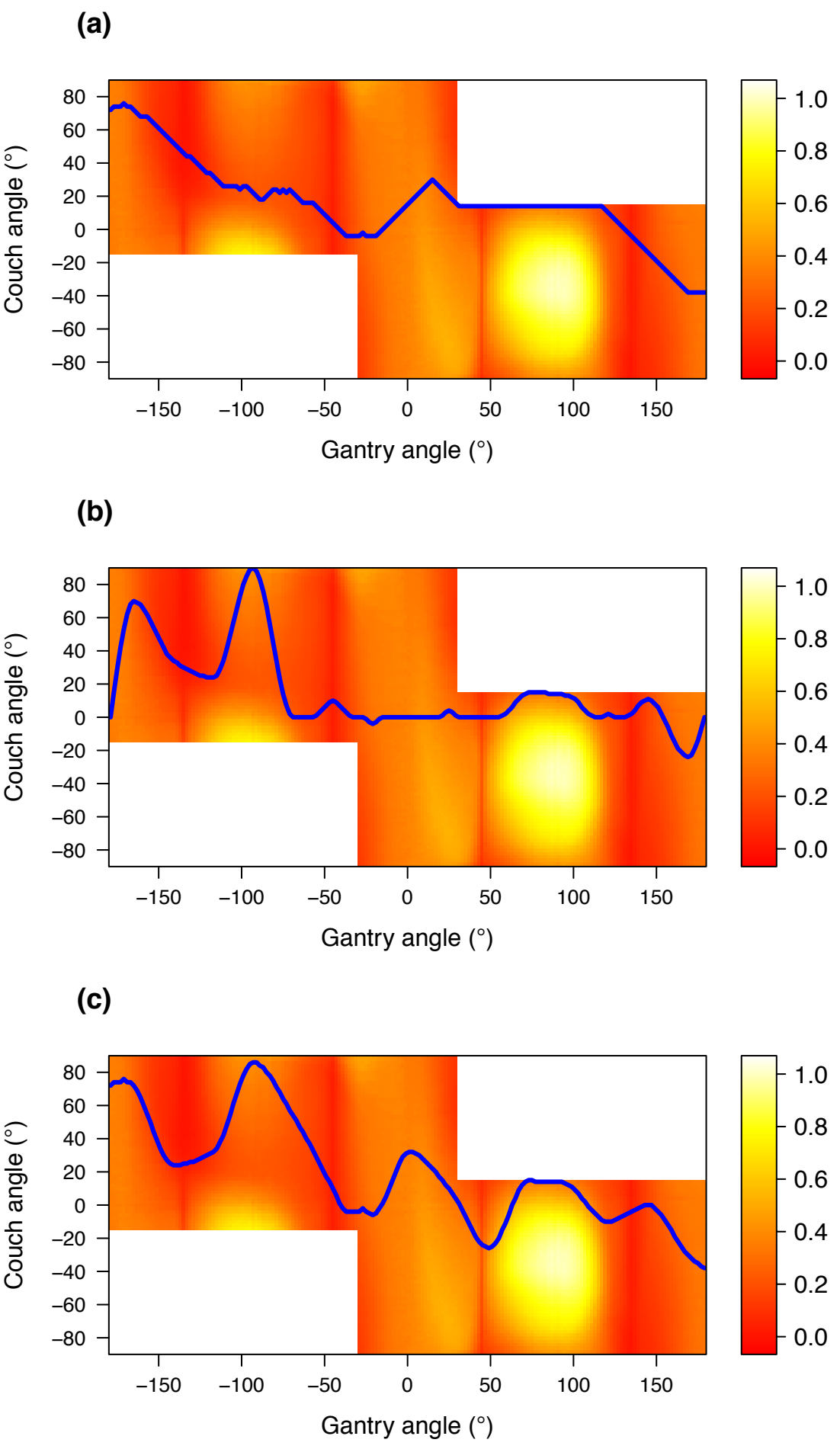
(a)
Couch angle (°)
80
60
40
20
0
−20
−40
−60
−80
−150
−100
−50
0
50
100
150
Gantry angle (°)
1.0
0.8
0.6
0.4
0.2
0.0
(b)
Couch angle (°)
Gantry angle (°)
(c)
Couch angle (°)
Gantry angle (°)

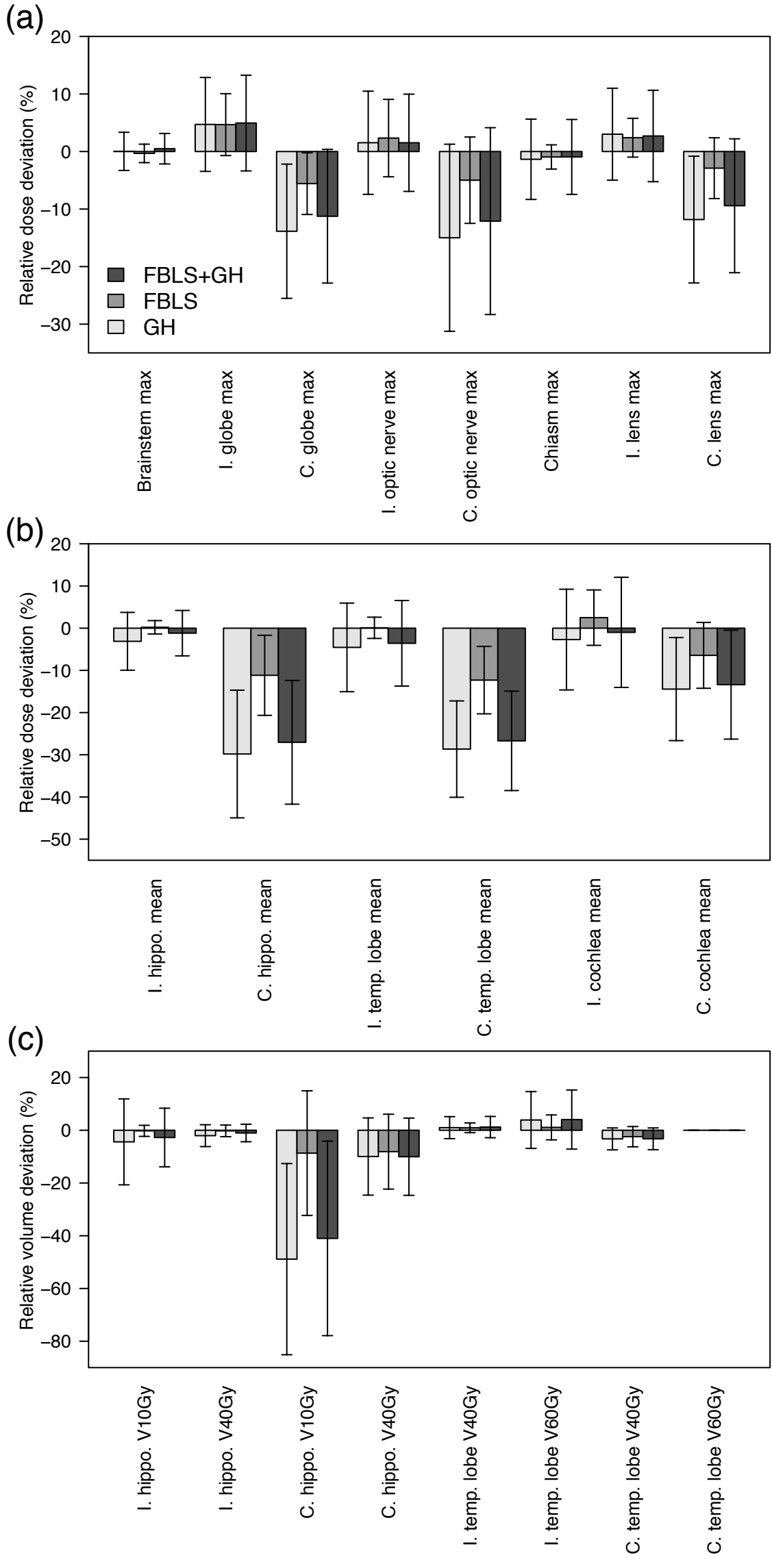
(a)
Relative dose deviation (%)
20
10
0
−10
−20
−30
FBLS+GH
FBLS
GH
Brainstem max
I. globe max
C. globe max
I. optic nerve max
C. optic nerve max
Chiasm max
I. lens max
C. lens max
(b)
Relative dose deviation (%)
20
10
0
−10
−20
−30
−40
−50
I. hippo. mean
C. hippo. mean
I. temp. lobe mean
C. temp. lobe mean
I. cochlea mean
C. cochlea mean
(c)
Relative volume deviation (%)
20
0
−20
−40
−60
−80
I. hippo. V10Gy
I. hippo. V40Gy
C. hippo. V10Gy
C. hippo. V40Gy
I. temp. lobe V40Gy
I. temp. lobe V60Gy
C. temp. lobe V40Gy
C. temp. lobe V60Gy

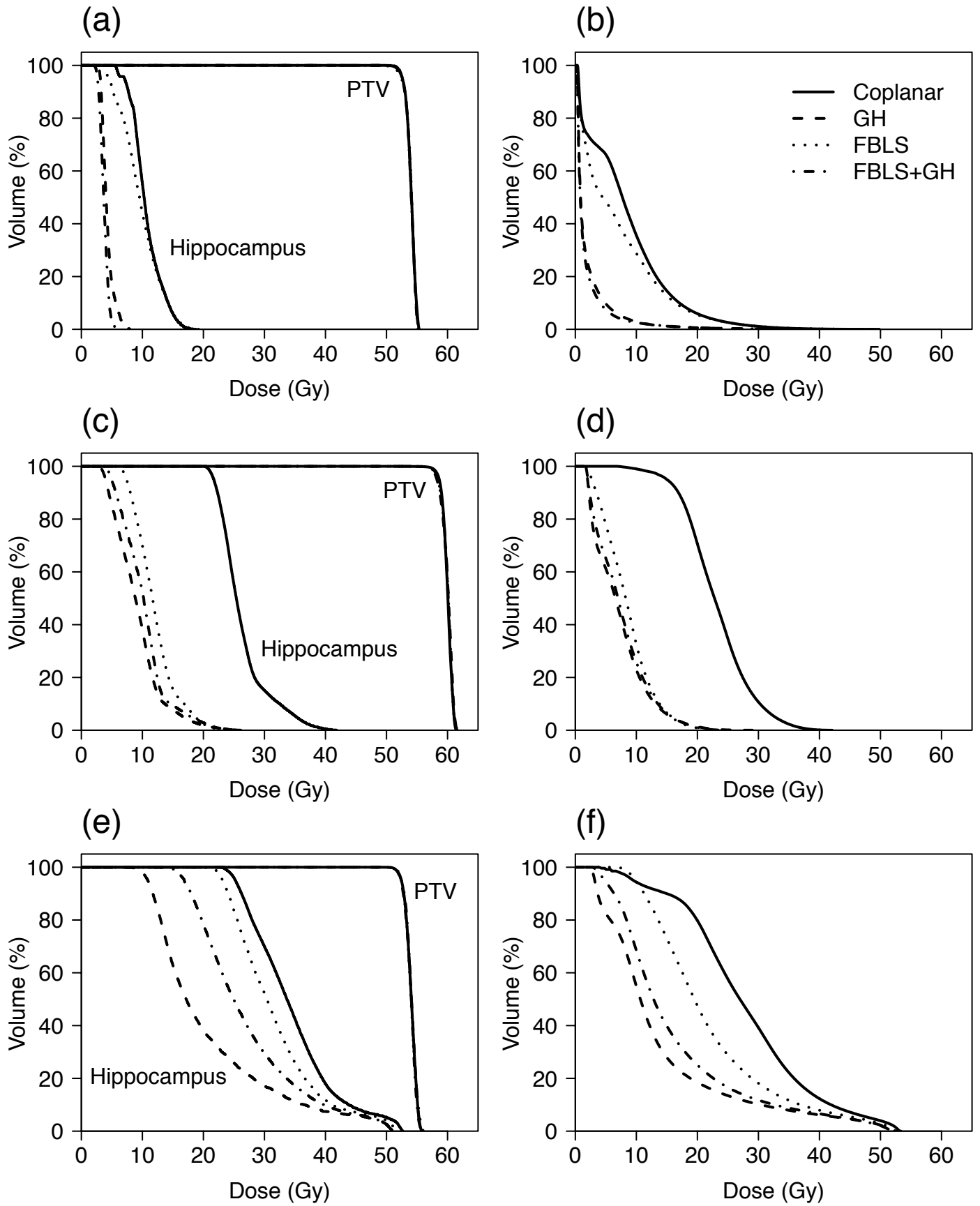
(a)
(b)
(c)
(d)
(e)
(f)
PTV
Hippocampus
Coplanar
GH
FBLS
FBLS+GH
Volume (%)
Dose (Gy)
0
20
40
60
80
100
0
10
20
30
40
50
60

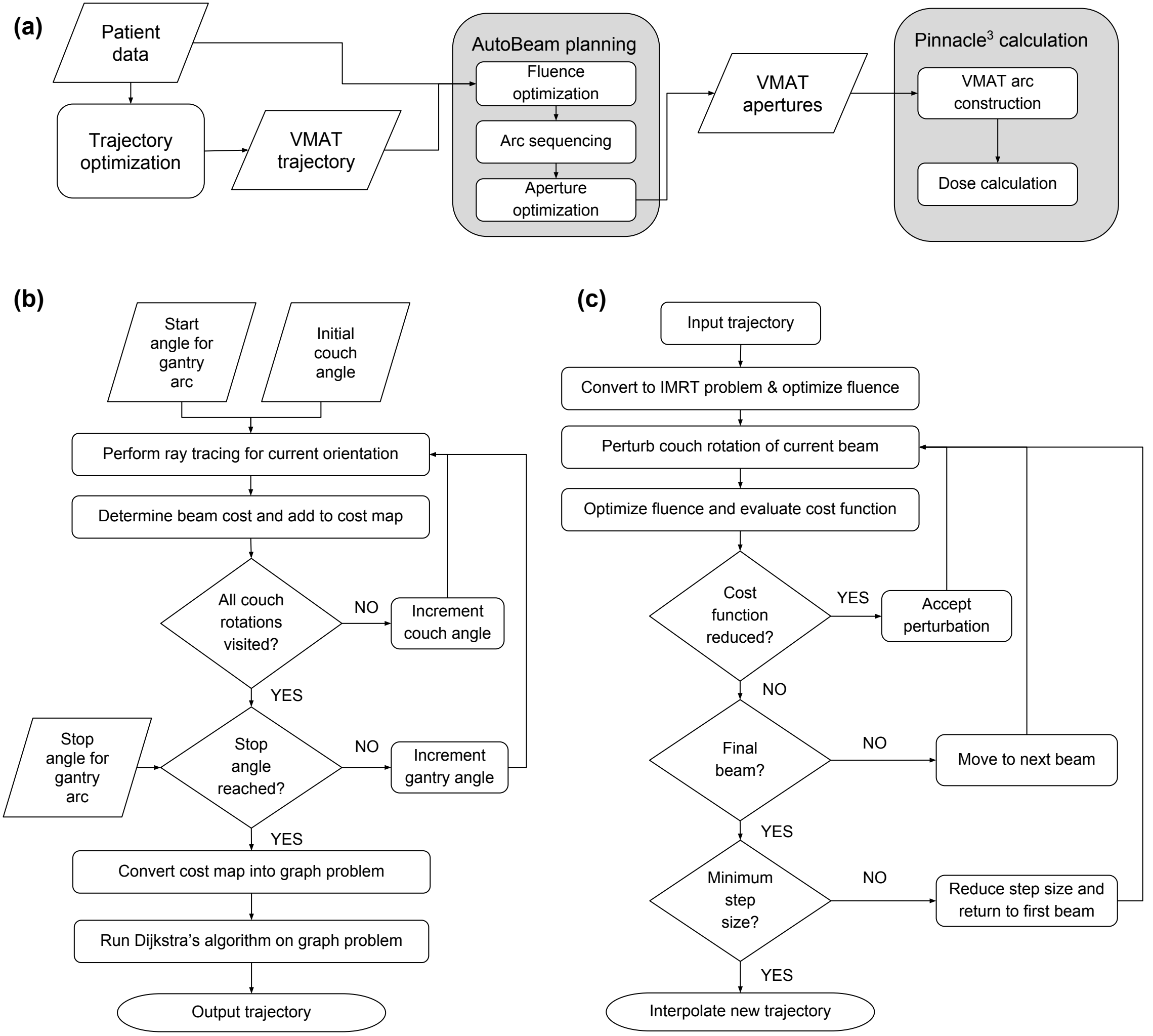

Figure A1. Flowchart showing (a) the non-coplanar trajectory planning workflow, (b) the geometric heuristic technique, and (c) the fluence-based local search algorithm.

Case	Diagnosis	Age at diagnosis (yrs)	PTV volume (cc)	Mean PTV dose (Gy)
1	Craniopharyngioma	21	5.5	54
2	Craniopharyngioma	16	31.7	54
3	Oligoastrocytoma	48	554.2	54
4	Astrocytoma	46	505.6	54
5	Astrocytoma	9	151.2	54
6	Glioblastoma	34	309.2	60
7	Glioblastoma	69	502.3	60
8	Glioblastoma	41	279.7	60
9	Glioma	79	271.0	60*
10	Astrocytoma	62	572.6	59.4
11	Glioneural tumour	18	84.2	54
12	Desmoplastic ganglioglioma	4	237.7	54
13	Glioblastoma	63	368.7	60
14	Glioma	42	451.8	60
15	Glioma	37	723.6	54

Table A1. Summary of patient diagnoses and prescriptions.* = original prescription 30 Gy in 6 fractions.

Region of interest	Objective	Relative importance
PTV	Minimize RMS around prescription dose	100
Brainstem	Minimize maximum dose	10
Globes	Minimize maximum dose	5
Optic nerves	Minimize maximum dose	5
Optic chiasm	Minimize maximum dose	5
Lenses	Minimize mean dose	5
Hippocampi	Minimize mean dose	3
Temporal lobes	Minimize mean dose	2
Cochleae	Minimize mean dose	1
Brain excluding other ROIs	Minimize mean dose	1

Table A2. AutoBeam optimization parameters. RMS = root mean square deviation. ROI = region of interest. Lens mean dose, not maximum dose, is used during optimization in routine clinical VMAT planning at our centre.

Region of interest / metric	Statistic	Mean ± 1 S.D.	
		Single arc	Dual arc
	$D_{98\%}$ (Gy)	54.6 ± 3.0	54.6 ± 3.0
PTV	$D_{50\%}$ (Gy)	56.8 ± 3.1	56.9 ± 3.1
	$D_{2\%}$ (Gy)	58.2 ± 3.2	58.2 ± 3.2
Brainstem	D_{Max} (Gy)	54.7 ± 4.6	54.7 ± 4.7
	D_{Mean} (Gy)	29.3 ± 12.5	29.2 ± 12.5
Ipsi. Globe	D_{Max} (Gy)	25.0 ± 12.1	25.3 ± 12.2
	D_{Mean} (Gy)	**16.2 ± 7.7**	**16.5 ± 7.9**
Contra. Globe	D_{Max} (Gy)	19.3 ± 6.6	19.2 ± 6.7
	D_{Mean} (Gy)	13.3 ± 5.0	13.2 ± 5.0
Ipsi. Optic Nerve	D_{Max} (Gy)	41.9 ± 15.5	41.9 ± 15.5
	D_{Mean} (Gy)	29.9 ± 12.3	30.1 ± 12.4
Contra. Optic Nerve	D_{Max} (Gy)	**34.6 ± 13.6**	**34.2 ± 13.7**
	D_{Mean} (Gy)	22.3 ± 7.8	22.1 ± 7.9
Chiasm	D_{Max} (Gy)	51.2 ± 9.3	51.2 ± 9.3
Ipsi. Lens	D_{Max} (Gy)	**15.2 ± 7.3**	**15.5 ± 7.5**
	D_{Mean} (Gy)	**12.8 ± 6.5**	**13.1 ± 6.8**
Contra. Lens	D_{Max} (Gy)	13.2 ± 5.1	13.1 ± 5.2
	D_{Mean} (Gy)	11.1 ± 4.7	11.0 ± 4.8
Ipsi. Hippocampus	D_{Mean} (Gy)	46.7 ± 14.8	46.7 ± 14.7
	V_{10Gy} (%)	97.3 ± 9.4	97.5 ± 8.6
	V_{40Gy} (%)	74.0 ± 41.9	74.1 ± 41.9
Contra. Hippocampus	D_{Mean} (Gy)	**30.4 ± 9.5**	**29.9 ± 9.3**
	V_{10Gy} (%)	97.0 ± 11.5	97.1 ± 11.4
	V_{40Gy} (%)	**16.3 ± 22.2**	**14.7 ± 21.4**
Ipsi. Temporal Lobe	D_{Mean} (Gy)	41.5 ± 15.9	41.6 ± 15.9
	V_{40Gy} (%)	59.7 ± 38.2	59.8 ± 38.2
	V_{60Gy} (%)	12.0 ± 21.8	12.0 ± 21.6
Contra. Temporal Lobe	D_{Mean} (Gy)	**23.6 ± 7.2**	**23.0 ± 6.9**
	V_{40Gy} (%)	**5.0 ± 6.0**	**4.3 ± 5.7**
	V_{60Gy} (%)	0.0 ± 0.0	0.0 ± 0.0
Ipsi. Cochlea	D_{Mean} (Gy)	**27.8 ± 22.5**	**27.9 ± 22.5**
Contra. Cochlea	D_{Mean} (Gy)	12.9 ± 8.4	12.7 ± 8.2
Body excluding PTV	D_{Mean} (Gy)	**11.6 ± 4.2**	**11.5 ± 4.2**
Body	D_{1cc} (Gy)	58.4 ± 3.4	58.4 ± 3.4
Monitor units		**238.7 ± 15.7**	**238.9 ± 15.9**
Homogeneity index	(%)	6.308 ± 0.846	6.353 ± 0.790
Gradient index		**2.708 ± 0.700**	**2.692 ± 0.705**
Conformation number		0.791 ± 0.064	0.791 ± 0.065

Table A3. Mean and standard deviations of dose statistics for single and dual arc coplanar VMAT. Significant statistical comparisons ($p < 0.05$) are indicated in bold. Ipsi and contra = ipsilateral and contralateral. Dx = dose to volume x. VxGy = relative volume receiving x Gy.